applied sciences

MDPI

*Article*

# Properties and Durability of Cementitious Composites Incorporating Solid-Solid Phase Change Materials

**Yosra Rmili [1], Khadim Ndiaye [1,*], Lionel Plancher [1,2], Zine El Abidine Tahar [1], Annelise Cousture [1] and Yannick Melinge [3]**

[1] Laboratoire L2MGC, CY Cergy Paris University, 95031 Neuville-sur-Oise, France; yosra.rmili@etu.cyu.fr (Y.R.); lionel.plancher@u-cergy.fr (L.P.); zine-el-abidine.tahar@cyu.fr (Z.E.A.T.)
[2] Laboratoire GEC, CY Cergy Paris University, 1 Rue Descartes, 95000 Neuville-sur-Oise, France
[3] LRMH, CRC—MNHN, CNRS, Ministère de la Culture—UAR 3224, 77420 Champs sur Marne, France; yannick.melinge@culture.gouv.fr
* Correspondence: khadim.ndiaye@cyu.fr

**Abstract:** This paper investigates the properties and durability of cementitious composites incorporating solid-solid phase change materials (SS-PCM), an innovative heat storage material. Mortars with varying SS-PCM contents (0%, 5%, 10%, 15%) were formulated and characterized for rheological, structural, mechanical, and thermal properties. Durability assessment focused on volume stability (shrinkage), chemical stability (carbonation), and mechanical stability (over thermal cycles). Mortars with SS-PCM exhibited significant porosity and decreased mechanical strength with higher SS-PCM content. However, thermal insulation capacity increased proportionally. Notably, the material's shrinkage resistance rose with SS-PCM content, mitigating cracking issues. Despite faster carbonation kinetics in SS-PCM mortars, attributed to high porosity, carbonation appeared to enhance long-term mechanical performance by increasing compressive strength. Additionally, SS-PCM composites demonstrated superior stability over thermal cycles compared to reference mortars.

**Keywords:** cementitious materials; phase change materials; properties; durability; shrinkage; carbonation



**Citation:** Rmili, Y.; Ndiaye, K.; Plancher, L.; Tahar, Z.E.A.; Cousture, A.; Melinge, Y. Properties and Durability of Cementitious Composites Incorporating Solid-Solid Phase Change Materials. *Appl. Sci.* **2024**, *14*, 2040. https://doi.org/10.3390/app14052040

Academic Editor: Alberto Vomiero

Received: 31 December 2023
Revised: 4 February 2024
Accepted: 13 February 2024
Published: 29 February 2024



## 1. Introduction

Energy consumption is a real challenge nowadays, particularly in the building sector, representing a significant part of it [1]. That is why many studies have been interested in and are still interested in finding ways and solutions to save energy and reduce greenhouse gas emissions. In fact, solar energy is one of these solutions, but the problem of intermittency is imposed.

In this regard, storing and using renewable energy become an urgent need in order to reduce energy consumption and then to improve indoor thermal comfort [1–3]. The heat storage is the key technology to streamline energy consumption and improve energy efficiency by reducing the gap between energy available and demand in buildings. There are different types of heat storage as sensitive, latent, thermochemical or chemical [1]. Therefore, phase change materials (PCM) have been advanced as one of the potential solutions to meet some of these expectations. Indeed, cementitious materials incorporating PCM, improve the thermal comfort of building, by increasing its inertia, thus avoiding sudden changes in the indoor temperature [4–10]. In the current market, there is a range of commercialized encapsulated phase change materials (solid-liquid) developed by leading companies such as BASF, Climator, Cristopia, Dupont de Nemours, Rubitherm, and Winco Technologies. All these technologies use encapsulated paraffin (micronal) as solid liquid phase change materials (SL-PCM). However, three significant drawbacks arise when utilizing SL-PCM. Firstly, the flammability of paraffin must be noticed. The associated risk is particularly unconvinient with fire safety requirements within buildings [11]. Secondly, because of a transition to a liquid state, such PCM require encapsulation to prevent against the leakage

risk within the building material. The technologies for containment involve encapsulations, which can be intricate, costly, and energy-intensive. Thirdly, the presence of PCM in the cement matrix can cause sustainability problems such as the drop in their mechanical performance [2,4–16] and the appearance of cracking [1,3,14,17]. When PCM is added to the mix, it influences the mechanical and even thermal properties such as the thermal conductivity of concrete [16]. The decrease of compressive strength seems to be more pronounced than that of tensile strength [18]. The volume instability of these SL-PCM generated durability problems (cracking, etc.) constraining their use in the building sector despite their energy efficiency. To address these challenges, solid solid phase change material (SS-PCM) with crystalline to amorphous conversion while remaining at a solid state, have been developed [19–23]. Among these researchers, Harlé et al. [23] has been developing several SS-PCM including the innovative PUX1520 used in this work. This SS-MCP exhibits interesting and relevant physical and thermal properties (89 $J.g^{-1}$ at 22 °C). for applications in the building sector. The solid liquid phase change of SL-PCM consists in endothermic melting during the heat charging phase and exothermic crystallization during the heat discharging phase. Solid solid phase change of SS-PCM undergoes a microstructural phase change from crystalline to amorphous while remaining at a solid state. This is referred to as the charging process. Conversely, when the temperature decreases, the SS-PCM releases heat as it crystallizes again, undergoing the discharging process (reversible conversion). The SS-PCM, more stable than SL-PCM, should be more suitable for building applications (masonry coating, bricks, roof coating, covering panels, etc.).

The innovative poly (ether urethane) based SS-PCM PUX1520 has interesting physical and thermal properties that are relevant for building applications [23,24]. Its integration in plaster has been the subject of preliminary studies [23], which have highlighted the interest and advantages of this technology SS-PCM compared with SL-MCP. They showed the high thermal inertia of Plaster/SS-PCM composites. The rheological properties in mortars are studied [24].

However, there is not study about the volume stability (shrinkage) and chemical stability (carbonation) of mortars incorporating this SS-MCP. Research on the durability of cementitious materials incorporating SS-PCM is very limited, which hinders their use in the building sector despite their energy efficiency. To use it as a construction material capable of storing heat, it is necessary to first study its properties and stability. The objective of this paper is to characterize and investigate the durability of cementitious materials incorporated the innovative SS-PCM to improve the thermal inertia of buildings. Furthermore, the effect of SS-PCM addition on the properties of cementitious materials (rheological, structural, thermal and mechanical properties) was studied on the one hand. On the other hand, since durability is a significant criterion for the use of building materials, the evaluation of their volume stability (drying shrinkage), chemical stability (accelerated carbonation) and finally mechanical stability (accelerated aging test over thermal cycles) was measured.

## 2. Materials and Methods

### 2.1. Materials

The SS-PCM composite mortars were prepared from white Portland CEM I 52.5 N cement containing 95%. The cement characterized by a Blaine specific surface 4200 $cm^2.g^{-1}$ is chemically composed by 74% $C_3S$, 12% $C_2S$, 11% $C_3A$ and 2.7% $SO_3$. The detail of the chemical composition is provided in the Table 1.

**Table 1.** Chemical composition of white cement.

| Oxide | $SiO_2$ | $Al_2O_3$ | CaO | MgO | $SO_3$ | $K_2O$ | $Na_2O$ | $Fe_2O_3$ |
|---|---|---|---|---|---|---|---|---|
| % | 21.53 | 3.59 | 65.47 | 0.70 | 3.49 | 0.26 | 0.6 | 0.22 |

The SS-PCM PUX1520 is an innovative poly (ether urethane) based SS-PCM developed by Harlé et al. [23,24]. Such home made SS-PCM is characterized by a high heat storage capacity of 89 $J.g^{-1}$ with a low phase change temperature of 22.3 °C. Thanks to its high hardness (30 shore D), the SS-PCM seems to be suitable for cementitious materials applications. Nevertheless, the tested formula is water soluble. The thermal conductivity at room temperature is 0.231 $W.m^{-1}$. $K^{-1}$ suggesting a good thermal insulation capacity [23]. The synthesized SS-PCM was crushed and sieved in white powder form with a grain size range between 300 µm and 600 µm (Figure 1). The SS-PCM has a molar mass of 1500 $g.mol^{-1}$, a bulk density of 1200 $kg.m^{-3}$ and a true density of 450 $kg.m^{-3}$.

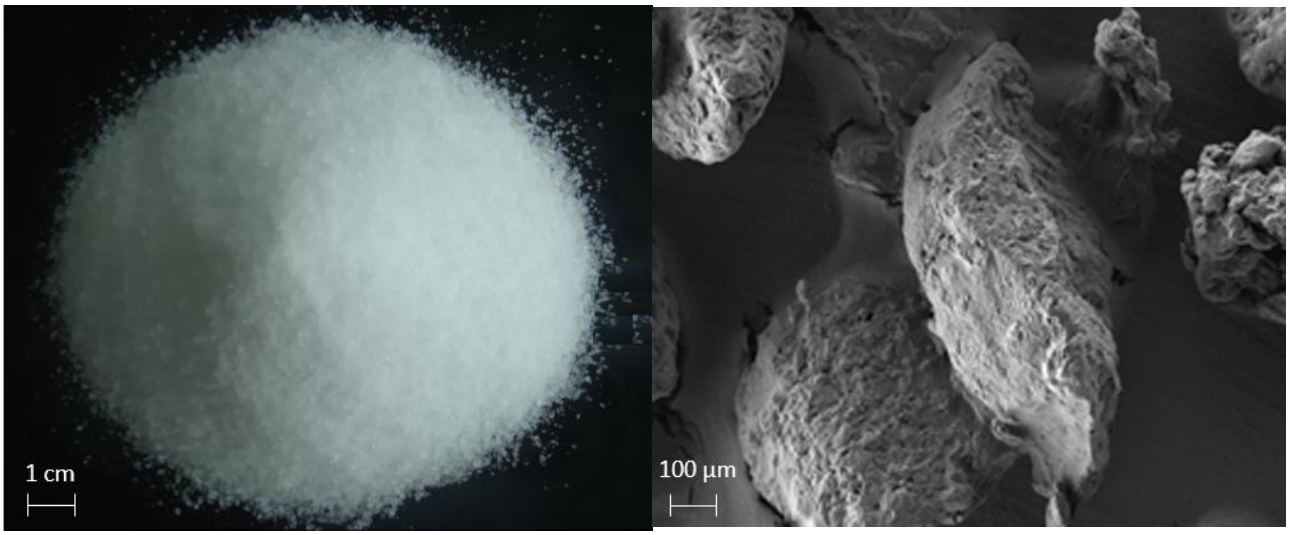


**Figure 1.** SS-PCM grains morphology: (**a**) macrostructure and (**b**) microstructure.

The SS-PCM composite mortars studied in the present work, are formulated as it reported in Table 2. The mortars were prepared according to the protocol described in Section 2.2. The cement-water ratio (W/C) has been fixed to 0.5 for all mix-designs. The mortar M0 is the reference sample without SS-PCM. The SS-PCM mortar composites M5, M10 and M15 contained addition of 5%, 10% and 15% of SS-PCM (SS-PCM in %wt mass of cement replaced in sand), respectively. The comparison between SS-PCM composite mortars and the reference mortar allows showing the SS-PCM addition effects.

**Table 2.** Composition of mortars.

| Mortars | SS-PCM (%wt Cement) | Water/Cement | Cement ($kg.m^{-3}$) | Water ($kg.m^{-3}$) | Sand ($kg.m^{-3}$) | SS-PCM ($kg.m^{-3}$) |
|---|---|---|---|---|---|---|
| M0 | 0 | 0.5 | 512 | 256 | 1535 | 0 |
| M5 | 5 | 0.5 | 503 | 251 | 1483 | 25 |
| M10 | 10 | 0.5 | 494 | 247 | 1433 | 49 |
| M15 | 15 | 0.5 | 486 | 243 | 1385 | 73 |

## *2.2. Methods*

### 2.2.1. Sample Preparation

The mixture of the mortars was ensured by the standard mixer NF EN 196-1 [25]. The cement and SS-PCM were mixed at a slow speed during 60 s to obtain a homogenous mixture (the cement only was mixed for M0). Then, sand was added and mixed at a slow speed during 30 s. Water is then added according to the fixed cement-water ratio of 0.5. After mixing during 30 s (slow speed), a stop time of 60 s is taken to scrape the bottom of the mixer bowl and left to be mixed for the next 60 s at high speed. The prepared mortars

were cast in prism molds (4 × 4 × 16 $cm^3$), and placed on a vibrating table. The vibration during 2 min allowed to ensure uniform thickness and to remove the air entrapped in the samples. This same mixing process was used for all formulations. The samples were stored in sealed bags at 20 °C and 100% relative humidity for 28 days. Finally, the mechanical and microstructure properties were determined after 28 days of moist curing.

#### 2.2.2. Analytical Techniques

The mortar workability was studied using a mini-slump test [26]. It was carried out using a metal mold in the form of a truncated steel cone with a height of 60 mm, a base diameter of 100 mm, and a top diameter of 70 mm. The mold was placed on a smooth, level surface, then filled with mortar in 3 layers. Each layer was tamped with stokes throughout its depth. The steel mold was removed from the mortar immediately by raising it slowly and carefully in a vertical direction. This allows the mortar to spread over the level surface. Then, the slump and the spread diameter were measured.

The flexural and compressive strength were measured with a 3R Quantech device at 28 days using 3 samples (4 × 4 × 16 $cm^3$) for each mix-design mortar. The tests were performed in accordance with standard NF EN 196-1 [25], with loading speeds of 50 and 2400 $N.s^{-1}$ for flexural and compressive strength tests, respectively. The resulting flexural and compressive strength values were the means of three and six individual values, respectively.

The microstructure of mortars was observed using a Gemini 300 (ZEISS) Scanning Electron Microscope (SEM) under high vacuum, with a working distance of 9 mm and a low voltage (2 kV) to avoid sample coating.

Mercury intrusion porosimetry (MIP) has been widely used to investigate the pore structure of cement-based materials. The pore distribution of composite samples (prism of 1 × 1 × 1 $cm^3$) was tested with the AutoPore IV 9500 device. Before testing, the samples were dried to remove air and water at 45 °C in a vacuum oven until a constant weight. The mercury pressure increasing allowed progressive access to the low porosity. The measured pore diameters were in the range of 0.003 µm to 358 µm.

The thermal conductivity and the thermal diffusivity have been identified with the use of a Hot-Disk device at 20 °C. The thermal properties was measured by the Transient Plane Source (TPS) methodology using prism samples (4 × 4 × 16 $cm^3$). The Hot-Disk probe was placed between two prepared surfaces of the prism samples. Finally, the specific heat was calculated from the measured thermal conductivity, thermal diffusivity and density. Before testing, the 28-day aged samples were oven-dried at 45 °C to remove the free water. Then, each sample was placed in a sealed bag and the cooling period was started at 20 °C. The free water has a significant influence on the measurements as water has its own thermal properties.

#### 2.2.3. Durability

The drying shrinkage of the prepared mortar samples (same preparation as in Section 2.2.1 but with different storage conditions) is estimated by weighting the samples and measuring their length. The different mortars were cast in metallic molds of 4 × 4 × 16 $cm^3$ previously equipped with two screws (i.e., incorporated in the mortar sample). After 24 h of hydration under autogenous conditions (into sealed bags), the specimens were removed from the mold. The mass loss of each sample was followed during water evaporation. A comparator (precision ± 0.002 mm) is used to manually measure the sample length of the sample over time. The initial measurement corresponded to 24 h after the mortar casting.

The accelerated carbonation testing was performed in a chamber at 3% $CO_2$, 20 °C and 65% RH according to PERFDUB protocol [27]. A prior drying process of samples has been done before the accelerated carbonation. Indeed, the 28 days aged mortar samples (4 × 4 × 16 $cm^3$) were dried in 45 °C oven during 14 days. Then a cooling period allows to prepare the specimens at 20 °C and 65% RH during 7 days [27]. After this drying process, the samples were placed into the accelerated carbonation chamber. The samples were

removed from the enclosure and weighed at 0, 14, 28, 48 and 360 days of carbonation. After that, the depth of carbonation was measured using a colored pH indicator (phenolphthalein). The phenolphthalein indicator was sprayed on the cutted surface (4 × 4 $cm^2$) to determine the carbonation depth.

The thermal stability of PCM mortars was followed by measuring their mechanical behavior after cycles thermally loading. The experimental protocol in terms of cycle time was previously set according to the thermal proprieties range of mortars in order to ensure the full spread of heat into the prism sample during a single considered cycle. The hygrometry was kept constant during the test. A monitored climate chamber is used to carry out the tests through 100 cycles. Each cycle of 5 h consisted of a heating step to 40 °C and a cooling step to 15 °C (Figure 2):

- Heating phase (heat charging): temperature increasing from 15 °C to 40 °C through a heating rate of 1 °C/min (for 25 min). After such heating period, the temperature is kept constant at 40 °C during 125 min.
- Cooling phase (heat discharging): temperature decreasing from 40 °C to 15 °C through a cooling rate of 1 °C/min (for 25 min). Finally after this cooling period, the temperature is kept constant at 15 °C during 125 min.

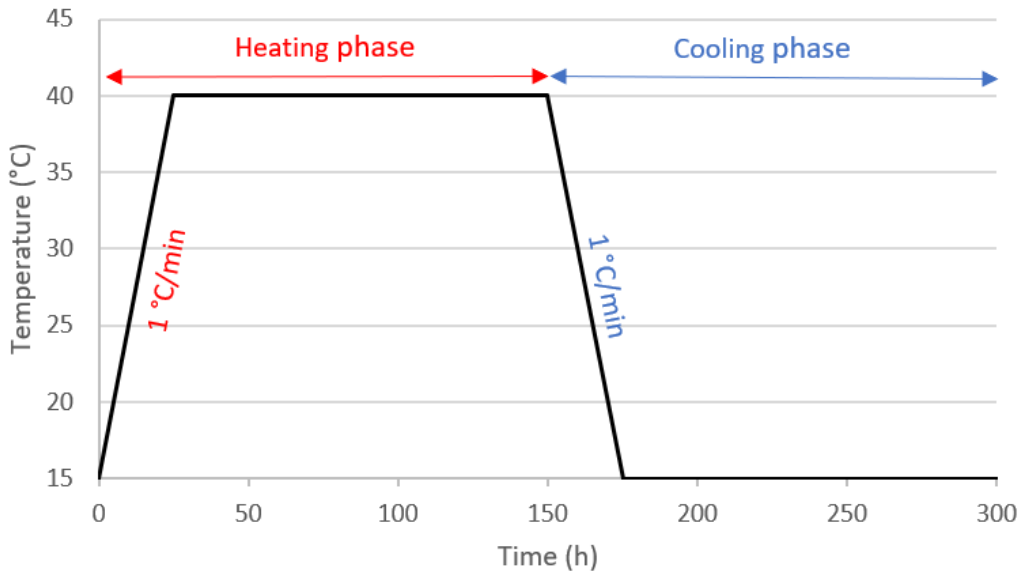


**Figure 2.** Set points of climate chamber temperature during a thermal cycle.

The mass variation of prism samples over time was followed by weighing specimens during cycles. The sample stability in terms of mechanical properties was evaluated by the measurement of their compressive strength over cycles.

## 3. Results

### *3.1. Mortar Proprieties*

The mortars M0, M5, M10 and M15 were characterized by the measurement of rheological, structural, mechanical and thermal properties using experimental protocols described in Section 2.2.

#### 3.1.1. Rheological Properties

In this study, the mini-slump test was used to evaluate the workability of cementitious materials incorporating SS-PCM and to get an idea of the influence of the different SS-PCM content on the rheological behavior of mortars (Figure 3). The reference mortar without SS-PCM shows lower workability with an average value of 3.3 cm for slump and about 13.3 cm for spread diameter. The slump and spread diameter increased with the added SS-PCM from 0% to 15%. That is to say, the SS-PCM added to the fresh mortar increased

its workability by fluidifying the mixture. The results obtained in the present work are in good agreement of those of Plancher et al. [24]. The noticed fluidification is induced both by the solubility of SS-PCM and by the non-cohesive granular effect which contributes to reduce the energy needed to shear the fresh suspensions. This visco-plastic behaviour is well described by the Herschel–Bulkley model [24]. Finally, such results indicate an ability of the SS-PCM to be used as a fluidifying agent in cementitious materials.

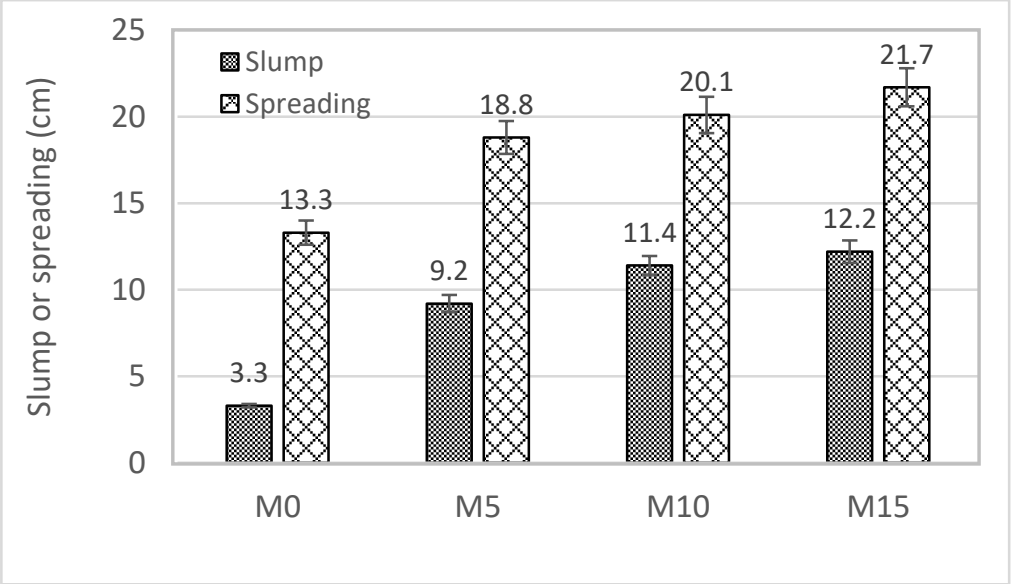


**Figure 3.** Slump and spread diameter of SS-PCM composite mortars.

3.1.2. Microstructure Properties

The effect of the SS-PCM incorporation on the hardened mortar microstructure was analyzed by scanning electron microscopic (SEM) observations (Figure 4). The morphology of 28 days aged mortars (M0, M5, M10 and M15) was observed for 2 scales: large field (a), and low field (b).

The observation of the large field images (a) shows clearly the macroporosity increasing with the SS-PCM incorporation. As a consequence, the SS-PCM addition should generate the modification of the pore size distribution. This should be confirmed by the mercury intrusion porosimetry test. The high macroporosity visible in M15 matrix (a) should have an effect on mechanical and thermal performance.

There is difference in morphology between M5, M10 and M15 noted in the low field images (b). Furthermore, Plancher et al. [24] observed the partial dissolution of SS-PCM in the cement paste during the mixing phase. This should generate chemical interactions between cement grains and soluble part of SS-PCM, which influences the cement hydration, hence the morphology. The centrifugation extraction of the interstitial fluid of the fresh mortar without (M0) and with SS-PCM (M5, M10 and M15), then ICP-OES analysis (Inductively Coupled Plasma Optical Emission spectroscopy) of extracted solutions would allow to quantity the dissolved part of SS-PCM in each fresh mortar.

The microstructure of M10 (low field), with needles sharped hydrates looking like ettringite, is very different to others mortars. There also seems to be C-S-H and ettringites phases visible in the M15 matrix. It is easier to distinguish hydrates in an aerated matrix, such as M15 matrix (less dense, less volume congestion). The hydrates in the other matrices (M0, M5, M10) are less visible because of their high density (volume congestion). Additional EDS on metallized samples are necessary to confirm the hydrate identification.

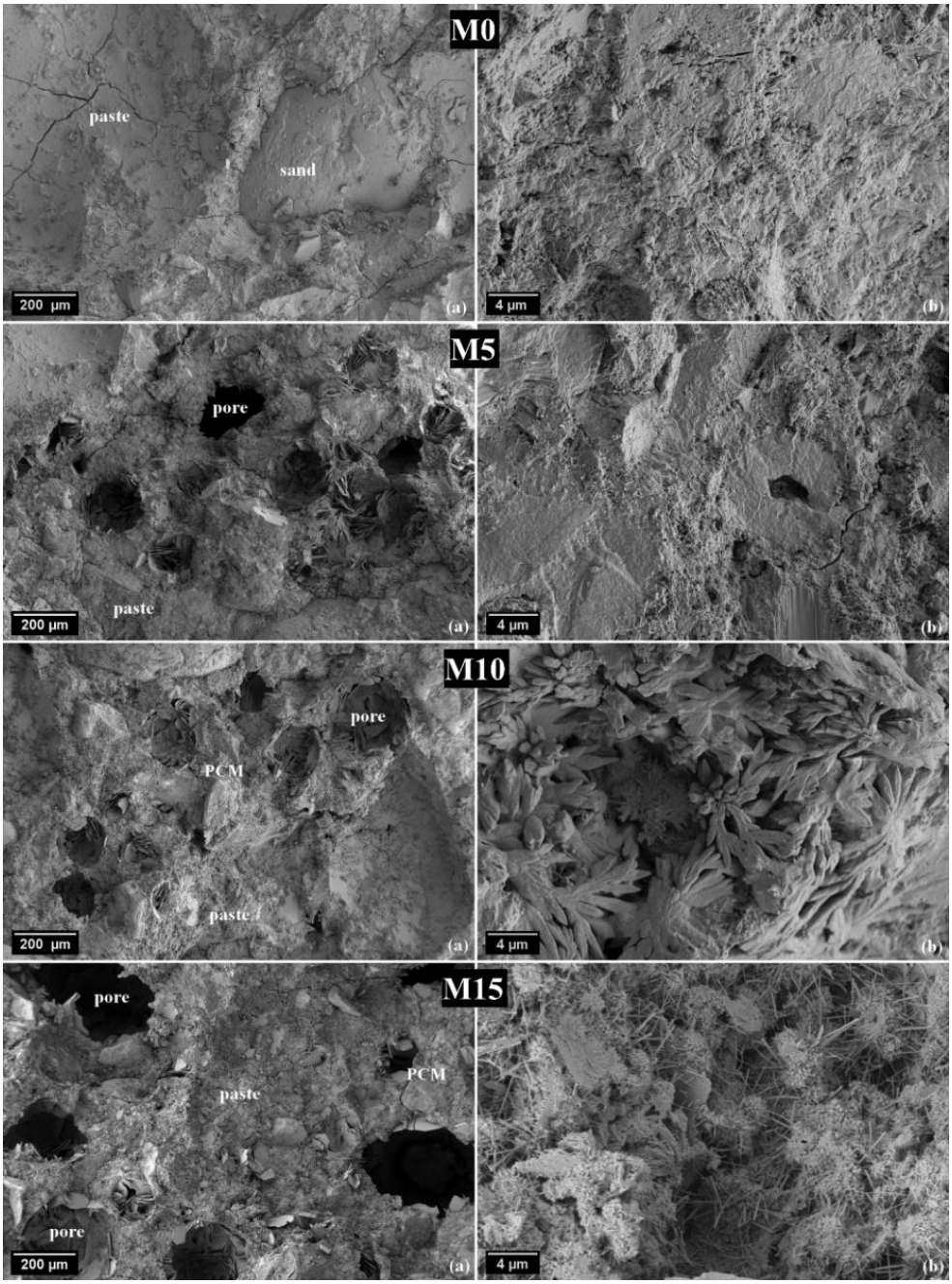


**Figure 4.** SEM Images of SS-PCM composite mortars after 28 days: (**a**) large field, and (**b**) low field.

### 3.1.3. Structural Properties

The porous structure network of mortars was investigated using Mercury Intrusion Porosimetry (MIP). It is by far the most widely used method to evaluate the size distributions of pores in cementitious materials, this is partially due to its wide range of pore size identification [28]. The Figure 5 shows the pore size structure of SS -PCM composite mortars with microporosity ($\leq$0.01 µm), mesoporosity (0.01–1 µm) and macroporosity ($\geq$1 µm). The mesoporosity of the reference mortar (1–100 µm) is represented by a single peak located at 10 µm. By considering the SS-PCM composite mortars, the access volume for the main mode (10 µm) is first reduced with the increasing incorporation of SS-PCM and a new pore size is created at around 60 µm. This new mode becomes more and more important via accessibility increasing induced by increasing the incorporation SS-PCM.

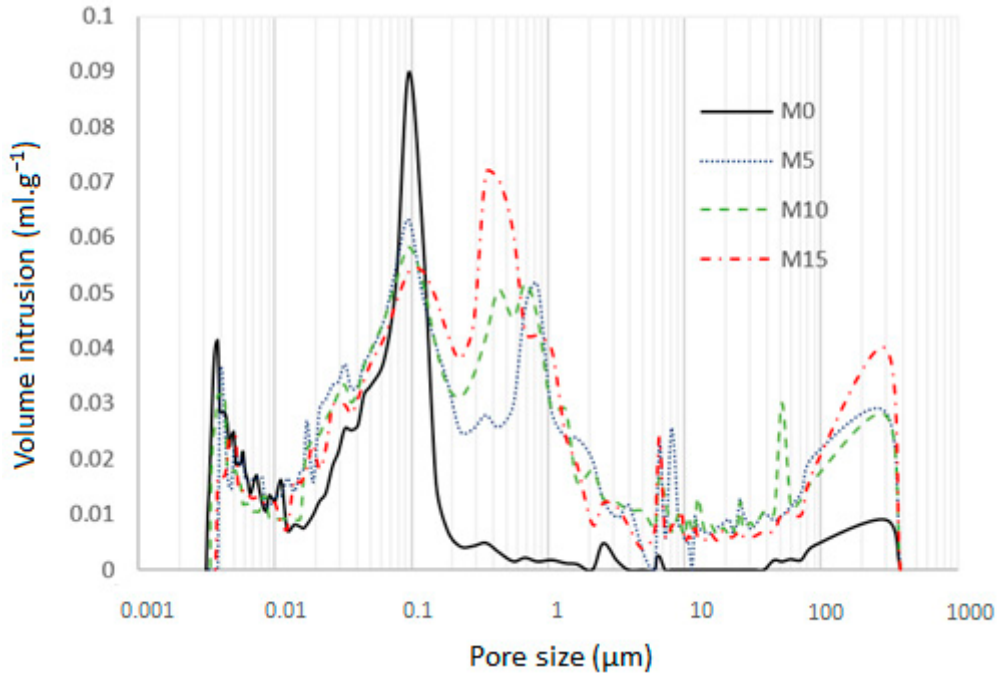


**Figure 5.** Pore size structure of SS-PCM composite mortars after 28 days.

The Figure 6 provides the pore size distribution of mortar porosity according to the mercury intrusion method. The total porosity of the mortars increased with the SS-PCM incorporation, because of the increase in macroporosity and mesoporosity, even if the microporosity decreased. The increase of macropores could be linked to the fact that the addition of SS-PCM leads to the decrease of the reactants content (cement and water), hence the drop of hydrates content into the mortar matrix leading to less dense matrix, and to more air content. As a consequence, for an equal amount of mortar, the cement paste content decreased with the SS-PCM addition. In addition, the sand grains were less bonded to each other (more pore voids between sand grains) because of the presence of SS-PCM grains without binding properties in the cement paste matrix. The decrease in microporosity should be related to the decrease of hydrate content with the SS-PCM addition (less cement and water content), knowing that the microporosity is related to the hydrate porosity. These results confirm the SEM observations in Section 3.1.2.

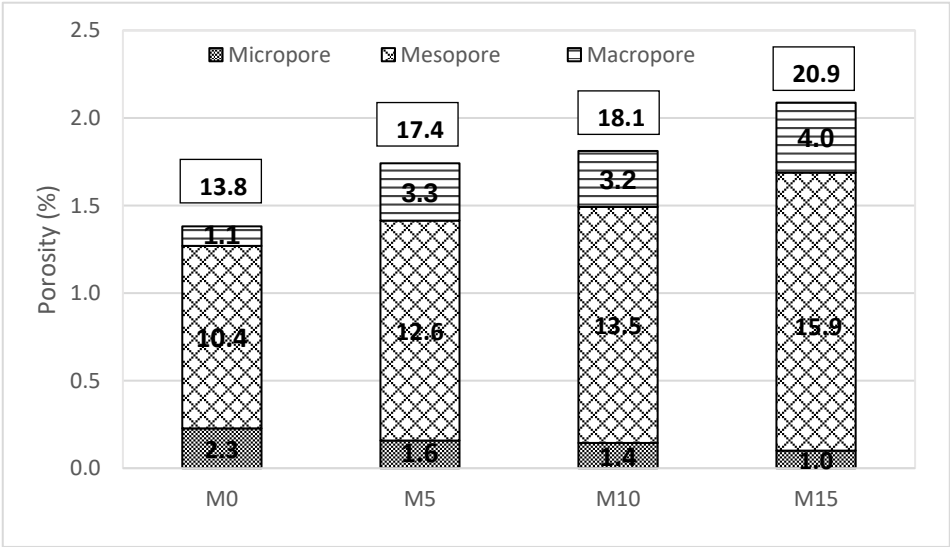


**Figure 6.** Pore size distribution of SS-PCM composite mortars after 28 days.

As expected, and in the opposite of porosity, the relative mass of SS-PCM increasing in the composites induced a functional decrease of the mortar density (Figure 7). This would induce modification of the construction material properties, such as mechanical or thermal performance.

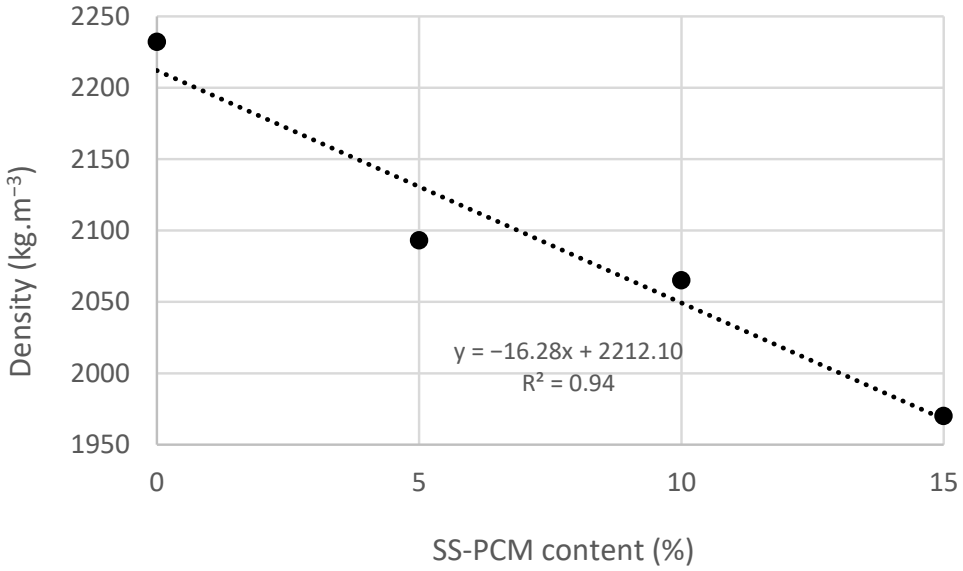


**Figure 7.** Density of mortars as a function of SS-PCM content of mortars.

### 3.1.4. Mechanical Properties

The flexural and compressive strengths were determined after 28 days of hydration to analyze the effects of SS-PCM incorporation on the mechanical properties of mortars. Figure 8 shows the results.

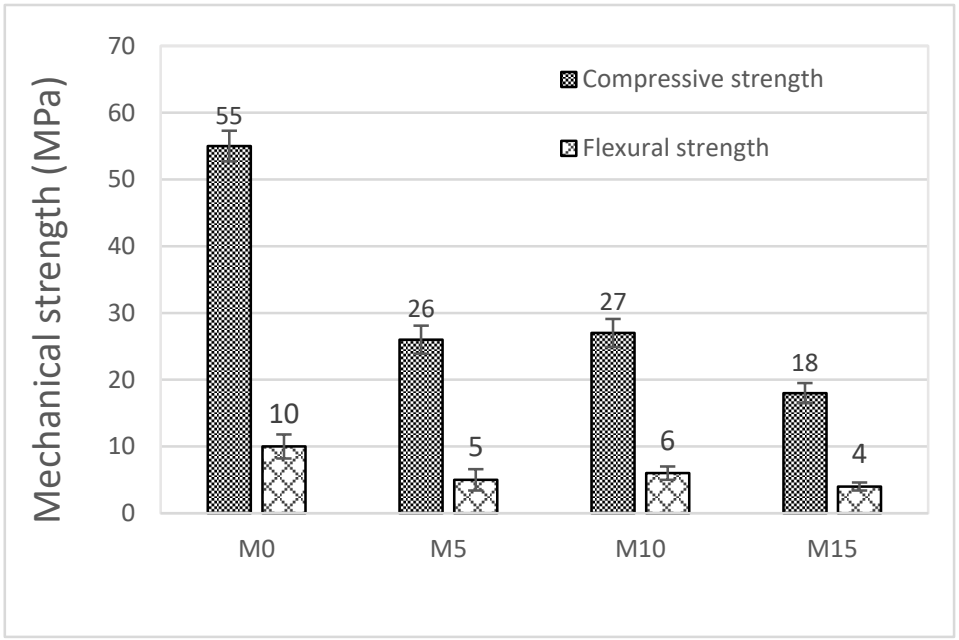


**Figure 8.** Mechanical strength of 28 days mortars as a function of SS-PCM content.

The flexural and compressive strengths of mortars incorporating SS-PCM were lower than those obtained for the reference mortar, and this reduction increased with the content of SS-PCM. There was a compressive strength drop of about 50% for the mortars M5 and M10, and 70% for M15%. These results are in agreement with the increase in mortar porosity

previously observed (Figures 5 and 6). It should be noted that the compressive strength of the M5 mortar was similar to that of the M10 mortar. As well as the total porosity, the M5 compressive strength (26 MPa) is very close to that of M10 (27 MPa). The Figure 8 shows a reduction in flexural strength of 50% between the reference mortar (M0) and SS-PCM composite mortars (M5, M10 and M15), and a similar compressive strength (around 5 MPa) between SS-PCM composite mortars (M5, M10 and M15).

The mechanical strength drop is a disadvantage for construction materials. However, the mechanical performance of SS-PCM composite mortars remains sufficient for most building applications (26 MPa for M5, 27 MPa for M10 and 18 MPa for M15). For building applications, in which higher mechanical is not needed (bricks, masonry wall, coating wall, roof panels) [2], the SS-PCM could be added to cementitious materials to improve the thermal performance of the building.

Thanks to review articles [2,29–31], the mechanical resistance of lightweight cementitious material and PCM cementitious material according to its density was provided in the Figure 9. The results of the present work were added to the figure as red squares. All results in the literature show a trend for the compressive strength to increase with the material density. However, for a given density, the mechanical strength differs according to the binder composition, foaming method and the hydration cure. This explains the wide dispersal of compressive strength according to the studies of lightweight materials. Our results (red squares) remain in the range of compressive strengths for PCM materials. The mechanical strength of PCM composites was lower than that of lightweight material for a given density. This is due to the presence of PCM molecules without binding properties in the PCM composite matrix. The advantage of PCM over lightweight aggregates is its latent enthalpy (heat storage capacity) providing high thermal inertia of building.

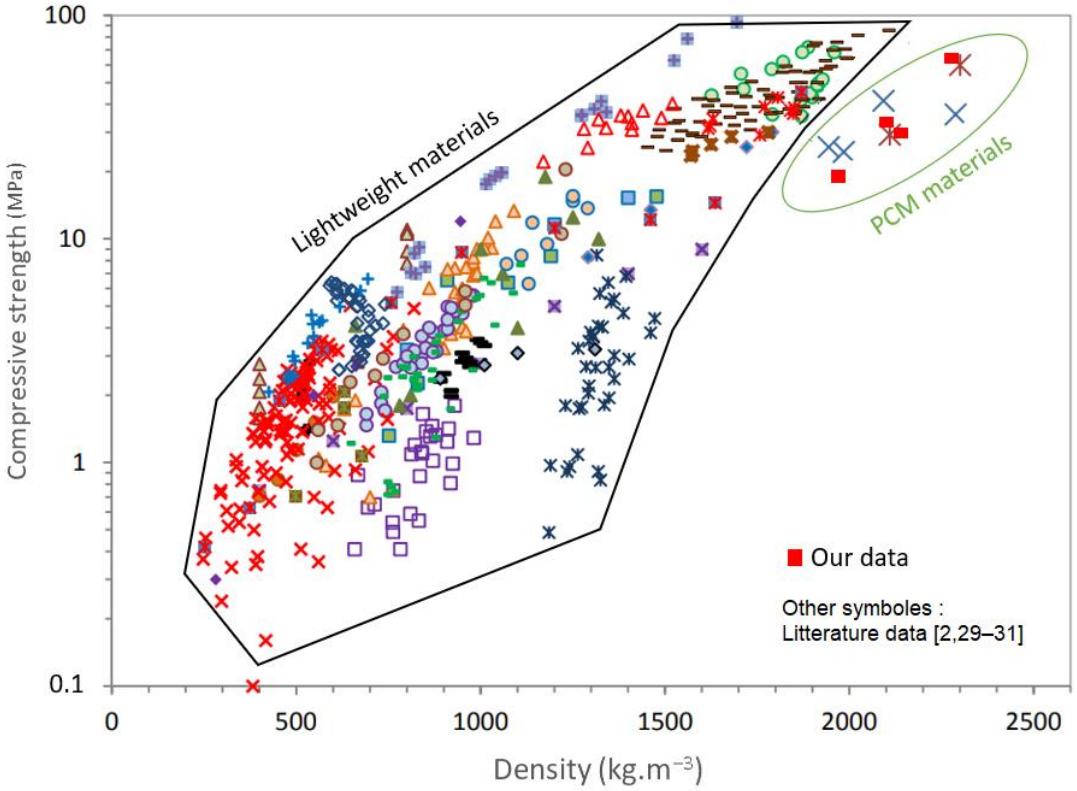


**Figure 9.** Compressive strength according to density [2,29–31].

### 3.1.5. Thermal Properties

The addition of 5% SS-PCM in the mortar led to a significant drop (26%) in terms of thermal conductivity. However, there was a slight variation in thermal conductivity among

the SS-PCM composite mortars (Figure 10a). The Figure 10b shows the rise of thermal conductivity with the porosity of mortars. Indeed, the thermal conductivity of cementitious materials depends on their air content. In addition, it should be noted that the low thermal conductivity of the added SS-PCM (0.231 $W.m^{-1}.K^{-1}$) promotes the high insulation capacity of mortar composites. The SS-PCM conductivity was about 7 times lower than that of the reference mortar. Unlike the mechanical strength decreased, the thermal conductivity drop is an advantage for building applications. The SS-PCM composite mortars have better thermal insulating capability compared to reference mortar, and seem suitable for low-energy buildings.

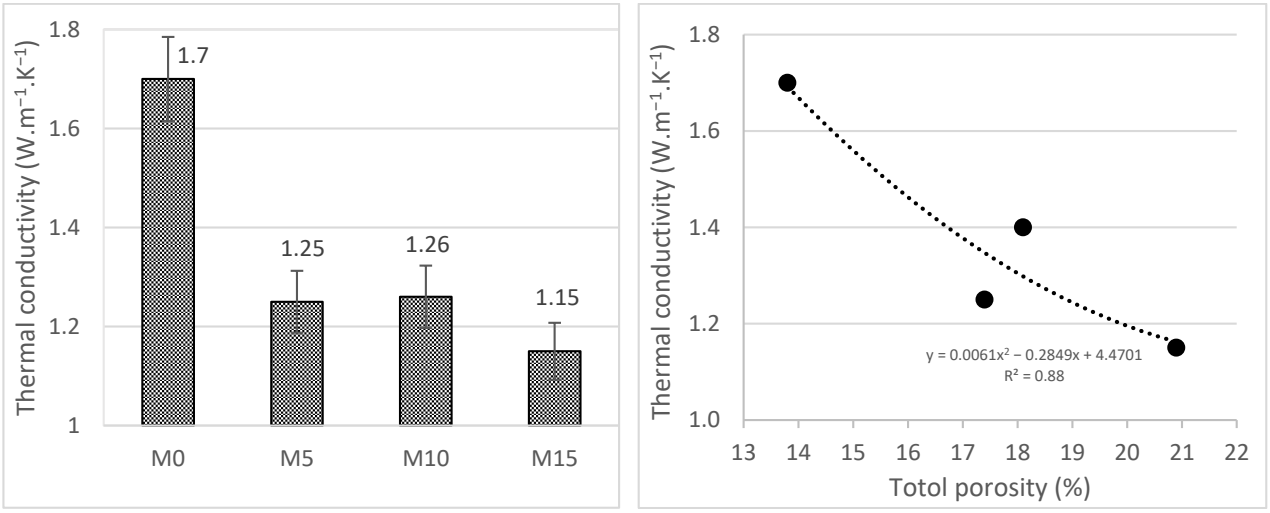


**Figure 10.** Thermal conductivity of mortars related to (**a**) SS-PCM content and to (**b**) porosity of mortars.

Unlike the compressive strength, the thermal conductivity of PCM composites was slightly lower than that of lightweight materials for a given density (Figure 11). This is due to the low thermal conductivity of the added PCM in the matrix. Our results (red squares) remain in the range of thermal conductivity for PCM materials. SS-PCM and lightweight materials are similar in terms of insulating capacity (similar thermal conductivity), but not in terms of thermal inertia. The advantage of SS-PCM over lightweight materials is its latent enthalpy, i.e., its high solar energy storage capacity providing high thermal inertia of building (unlike, the thermal inertia of lightweight material is low). In addition, the SS-PCM provides better durability and rheological properties. However, it should be noted that the lightweight materials are cheaper than PCM composites.

Unlike thermal conductivity, specific heat was higher when SS-PCM was added to mortar (Figure 12). In fact, the specific heat only depends on solid and phases of the mortar (i.e., cement paste, sand and SS-PCM), while the thermal conductivity takes into account all phases of the material (i.e., including the gas phase (porosity)). However, the specific heat of SS-PCM mortars was not a linear function of the SS-PCM amount.

The mechanical and thermal performances of SS-PCM composite mortars remain sufficient for most building applications. Moreover, its high thermal insulating capability and heat storage [23] are also relevant benefits for low-energy consumption buildings. This allows to improve the thermal inertia of the building, thus avoiding sudden changes in the indoor temperature, all while maintaining the supporting structure capacity. However, its higher porosity could lead to durability problems.

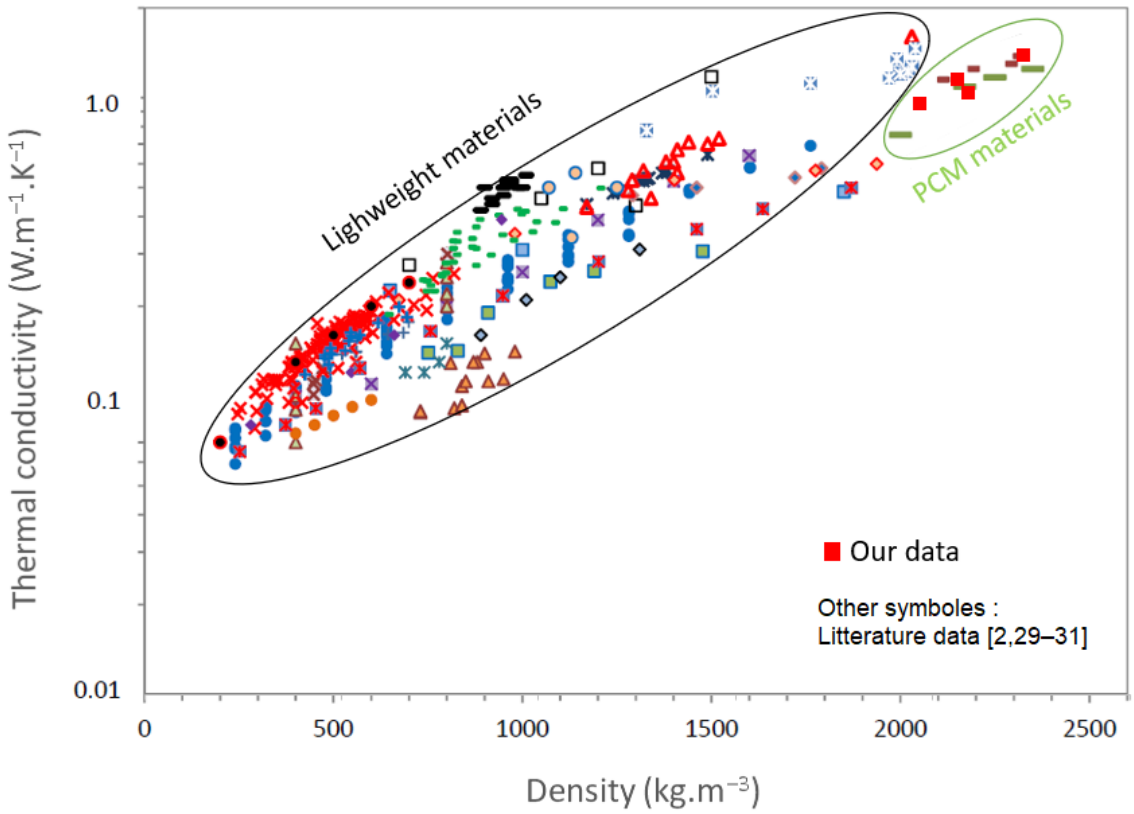


**Figure 11.** Thermal conductivity according to density [2,29–31].

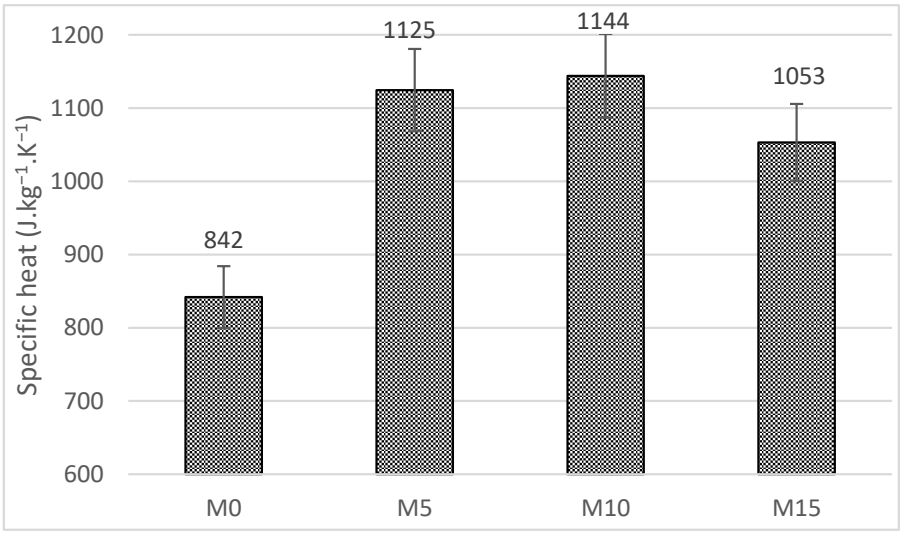


**Figure 12.** Specific heat of SS-PCM composite mortars.

### *3.2. Durability of Cementitious Composites Incorporating SS-PCM*

As durability is an essential criterion for building materials, the SS-PCM composite mortars stability was investigated. This aims to evaluate volume stability (shrinkage), chemical stability (carbonation) and mechanical stability over thermal cycles of SS-PCM mortars.

#### 3.2.1. Volume Stability: Drying Shrinkage

The drying shrinkage of cement-based materials can lead to structural cracking. In the literature, drying shrinkage is considered to be a consequence of changes in disjoining pressure, capillary pressure, and surface free energy or combinations thereof, accompanying

a decrease of saturation and internal relative humidity [32–35]. The capillary pressure in the pore network is the mechanism that is usually employed to describe the hydric strains in porous materials [35]. It is related to the formation of water-air menisci in the partially empty pores, which induce isotropic compressive stress within the rigid solid skeleton that leads to bulk shrinkage. The essential cause of drying shrinkage is, of course, the evaporation of the capillary water from the material surface exposed to the ambient air. Evaporation occurs as soon as the relative humidity of the ambient air is lower than that prevailing in the capillary network. The tension forces developed inside the concrete lead to its contraction. The SS-PCM effect on drying shrinkage of SS-PCM mortars is investigated.

The specimens of 24 h ($4 \times 4 \times 16$ cm$^3$) are removed from the molds, and placed in a climate chamber (20 °C and 50% RH). The mass evolution of each sample is followed during the water evaporation. Figure 13 shows the mass loss over time for each mix-design mortar. The water desorption kinetics was rapid in the short term, then the kinetics slowed down for all mortar samples (M0, M5, M10 and M15) after 20 days. The mass loss of water into the mortars increased with the SS-PCM content. This was related to the pore diameter and porosity which increased with SS-PCM content.

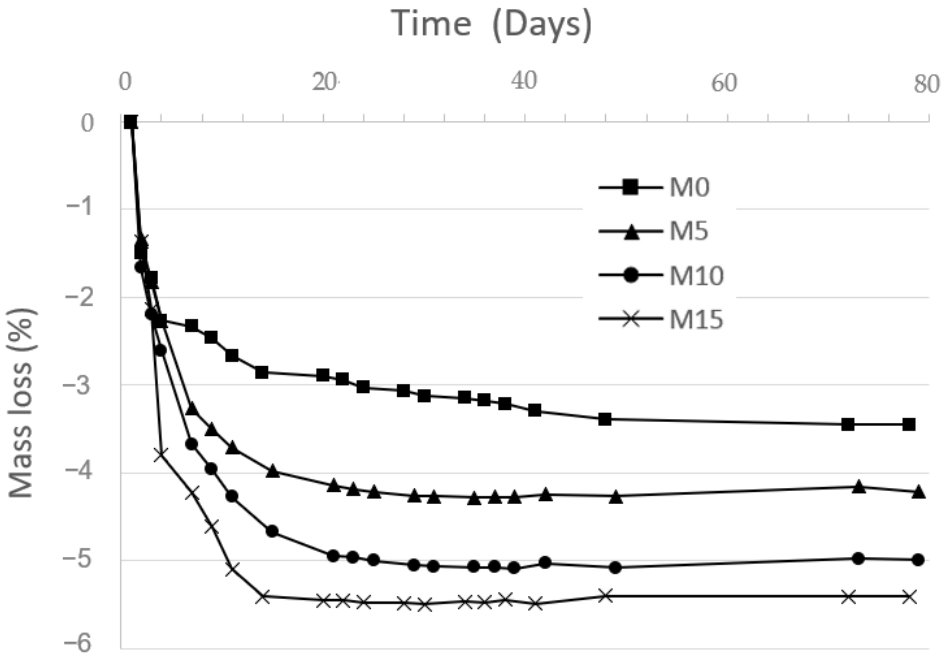


**Figure 13.** Mass loss of mortars over time.

Moreover, the capillary pressure, is related to the internal relative humidity according to the Kelvin–Laplace law [32]. So, the drying shrinkage amplitude should increase with the water loss [36]. However, it is noted that the SS-PCM addition generated more water loss (Figure 13), but less drying shrinkage (Figure 14). The incorporation of 5%, 10% and 15% of SS-PCM into the mortar allowed reducing the drying shrinkage amplitude by 7%, 42% and 53%, respectively. This should be related to the higher compressibility of the SS-PCM compared to cementitious materials able to amortize the drying shrinkage [19]. Therefore, the SS-PCM (grains size 300–600 µm) into the mortar matrix would amortize local stress due to the capillary pressure (generated by water loss) into the porous network, leading to less measurable bulk deformation of the skeleton. Hence, the addition of SS-PCM has the advantage of reducing macroscopic deformation linked to drying shrinkage.

Furthermore, it should be noted that shrinkage is probably the most common cause of structural cracking [37,38]. If not controlled, the deformation due to shrinkage can lead to durability problems and even shear stress [39,40]. The SS-PCM could be used as a mitigation agent to reduce the drying shrinkage of cementitious materials.

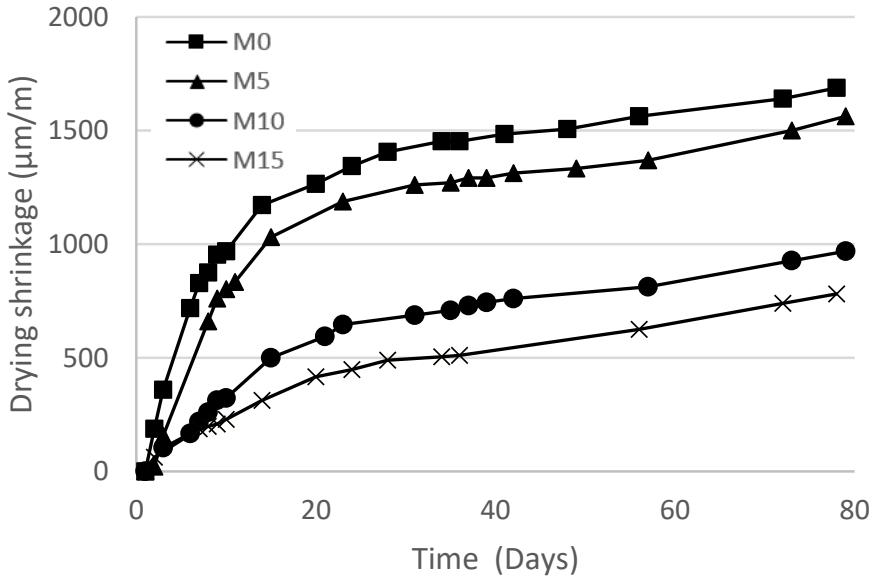


**Figure 14.** Drying shrinkage as a function of time.

3.2.2. Chemical Stability: Carbonation

Carbonation of concrete is a natural phenomenon that occurs in the long term in the ambient air. However, it is a slow process in atmospheric conditions taking a few years to reach high carbonation depth in the ambient air. The accelerated carbonation in a chamber at 3% $CO_2$ (20 °C and 65%RH) allows to speed up the process while maintaining stable environmental conditions according to the PERFDUB test method [27]. Figure 15 shows the evolution of the mass loss of mortar samples (4 × 4 × 16 $cm^3$) during the drying period at 45 °C before the carbonation test. The water loss is greater for mortars incorporating SS-PCM compared to the reference mortar. As seen before (Figure 13), the mass loss increases with SS-PCM content. This should be related to the high porosity of SS-PCM composites. After 14 days in 45 °C oven, the mortar samples were stabilized at 20 °C and 65% RH during 7 days (prior drying stage) [27]. They were then introduced into an accelerated carbonation chamber (3% $CO_2$, 20 °C and 65% RH).

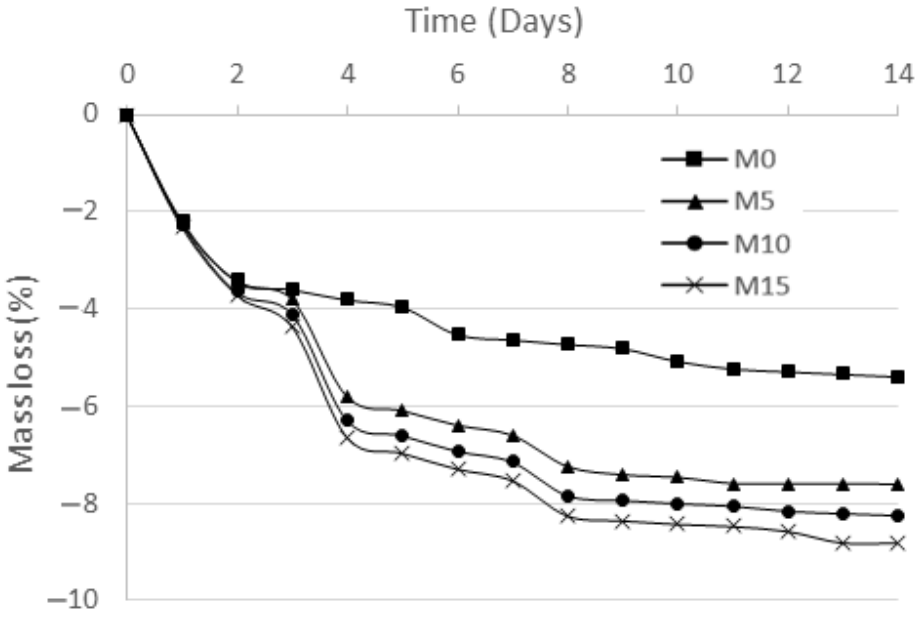


**Figure 15.** Mass loss of mortars over time in drying oven at 45 °C for 14 days.

The Figure 16 shows images of mortar samples after 14, 28, 48 and 360 days of accelerated carbonation. The phenolphthalein indicator was sprayed on the cutted surface to determine the carbonation depth. Phenolphthalein turns to purple coloration in area of pH higher than 9, so the purple coloration was observed in non-carbonated areas. The colorless outer area (carbonated area) thickened over time, i.e., the carbonation depth increased over time for all the tested mortars. At 360 days, the mortars with SS-PCM are fully colorless (i.e., complete carbonated).

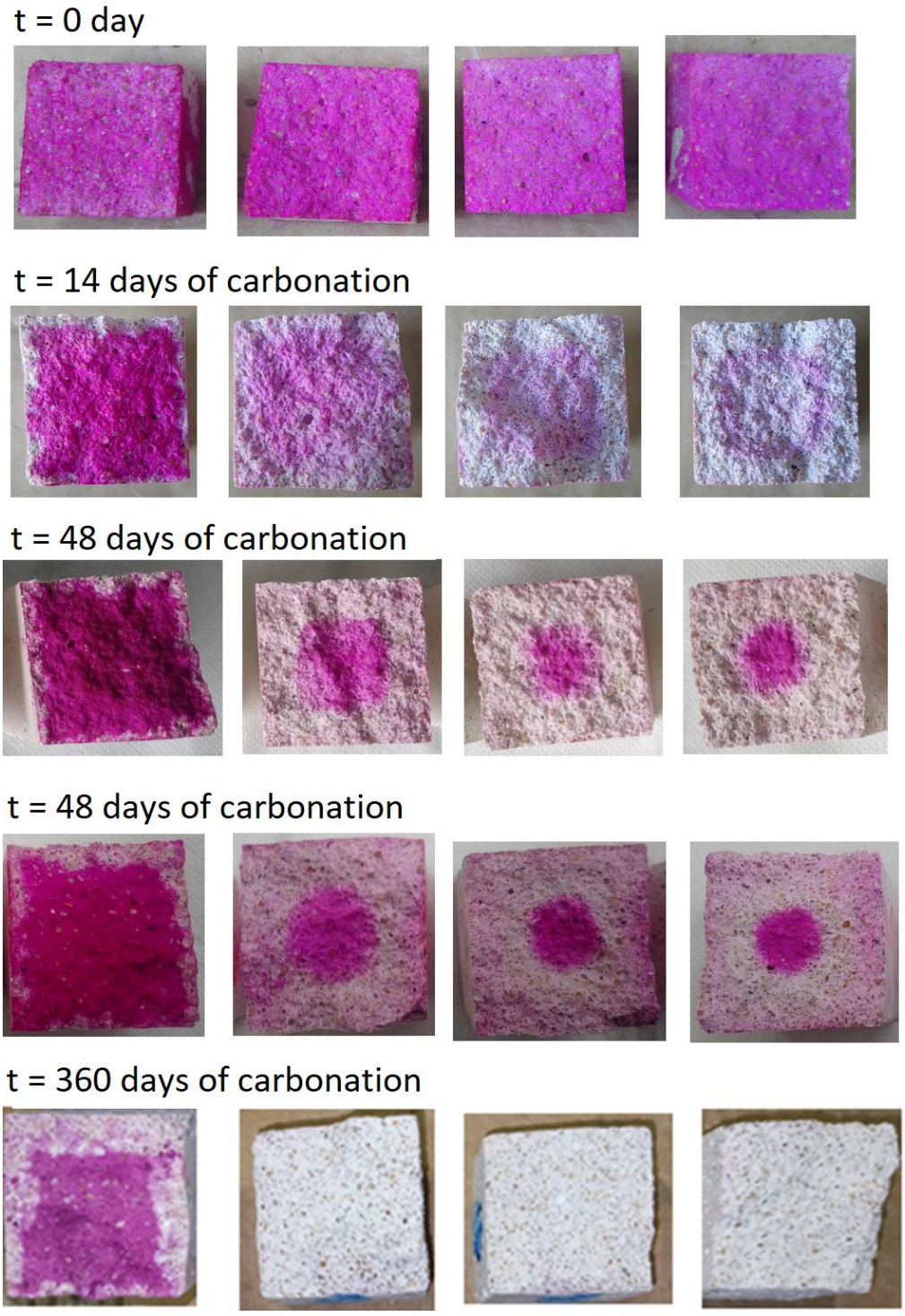


**Figure 16.** Image of SS-PCM composite mortars (4 × 4 $cm^2$) carbonated at 3% $CO_2$ chamber (20 °C, 65% RH).

Figure 17 shows the measurement of carbonation depth at 14, 28, 48 and 360 days for each mix-design mortar (M0, M5, M10 and M15). As seen in Figure 16, there was no carbonation at the beginning of accelerated carbonation (t = 0 day). Then, the carbonation depth at 14 days was observed and could be measured for all samples. The carbonation depth of all mix-design mortar increased over time. However, the carbonation kinetics of the reference mortar was slower compared to SS-PCM composite mortars. The carbonation kinetic increased with SS-PCM content. After 1 year of accelerated carbonation, the carbonation of mortars incorporating SS-PCM (M5, M10 and M15) was complete (≥20 mm), while that of reference mortar reached 6.8 mm. The high kinetic of SS-PCM composite mortars in relation to the reference mortar was due to its higher and coarser porosity, promoting a high diffusion of $CO_2$ into the porous network.

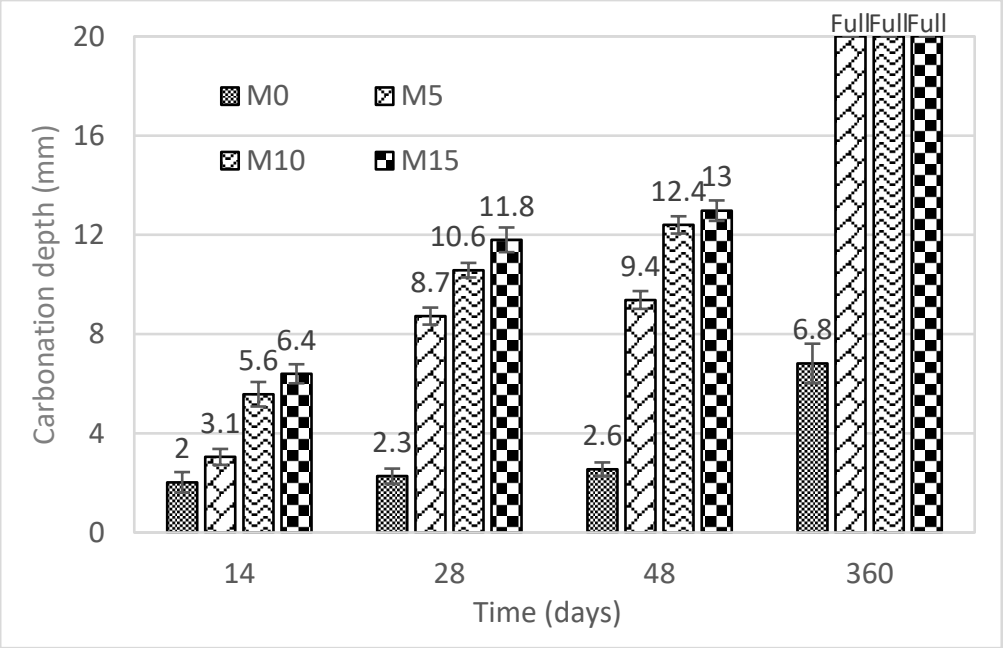


**Figure 17.** Carbonation depth of SS-PCM composite mortars over time.

It should be noted that the high carbonation depth of mortars incorporating SS-PCM is partially due to the severe carbonation conditions in the accelerated chamber (3%$CO_2$). In the real condition of use (building application), the carbonation kinetics in the atmospheric air was slower compared to the accelerated chamber. In fact, the Figure 18 shows the image of mortars carbonated for 360 days at atmospheric air chamber and accelerated carbonation chamber (3% $CO_2$). The SS-PCM composite mortars are fully carbonated in chamber at 3% $CO_2$ (≥20 mm), unlike those in the air atmospheric chamber.

In the atmospheric carbonation, the SS-PCM composite mortars show similar carbonation depth between 5 and 6 mm, while the reference mortar achieved only 1.7 mm in carbonation depth (Figure 19).

This high carbonation rate of SS-PCM composite mortar could be an advantage in term of mechanical performance. Figure 20 shows an increase in mechanical strength with the carbonation rate. Such a behavior can be related to effects induced by the carbonation that leads to the calcium carbonate precipitation into the porous network reducing the porosity, and improving the compressive strength. However, the low pH of carbonated mortars could promote the corrosion of steels for reinforced concrete [41]. The SS-PCM mortar should be suitable for non-reinforced concrete: masonry coating, masonry bricks, roof coating, covering panels, etc.

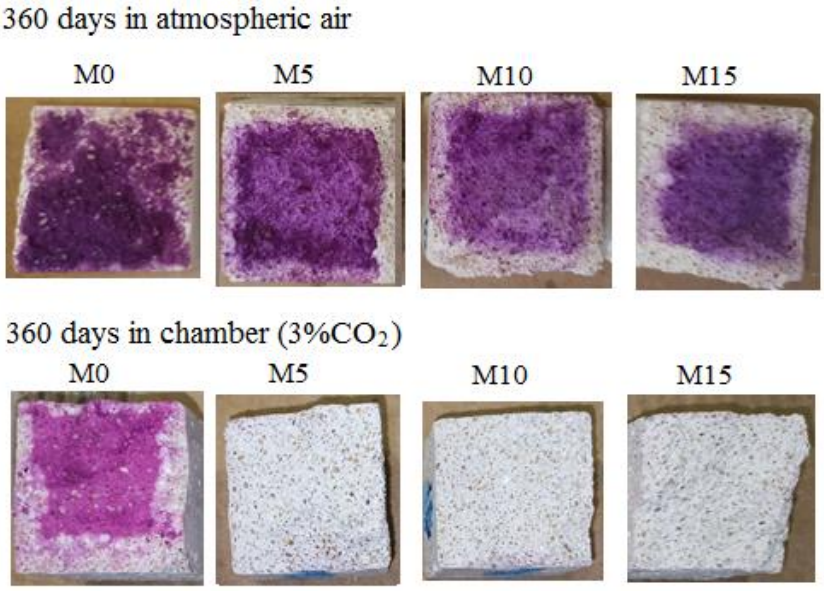


**Figure 18.** Images of carbonated mortars for one year in atmospheric air and in 3% $CO_2$ chamber.

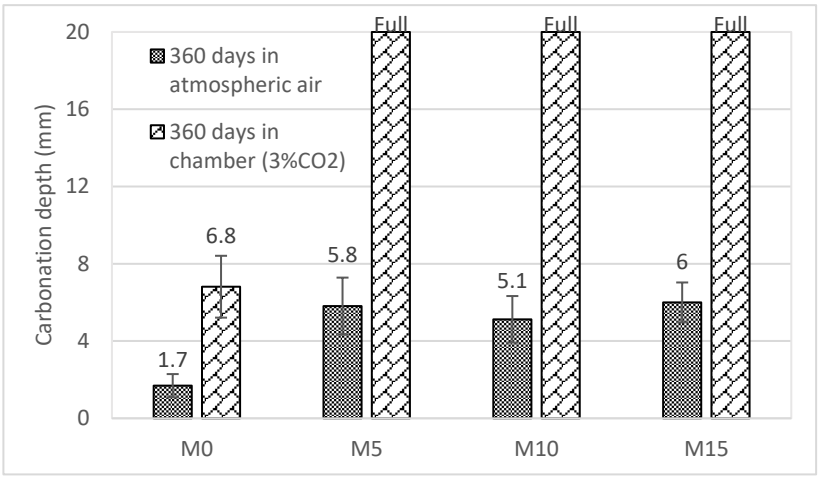


**Figure 19.** Carbonation depth of mortars for one year in atmospheric air and in 3% $CO_2$ chamber.

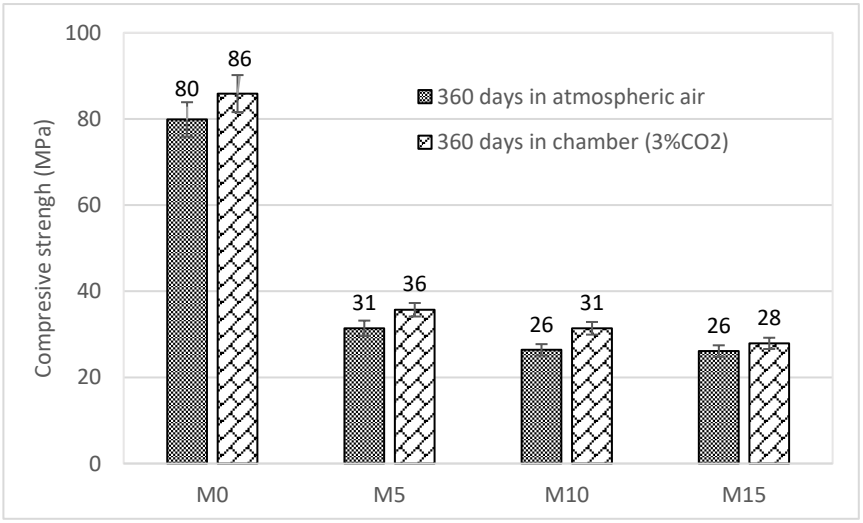


**Figure 20.** Compressive strength of carbonated mortars for one years.

3.2.3. Mechanical Stability: Reversibility over Thermal Cycles

It is relevant to check the stability of mortars incorporating SS-PCM over thermal cycles, or in other words its ability in terms of mechanical strength to withstand the SS-PCM phase transitions (heat storage) during the building lifespan. The heating at 40 °C and cooling at 15 °C led to charge and discharge heat into SS-PCM, respectively. The Figure 21 shows the results of the aging test in terms of compressive strength as a function of the number of phase transition cycles (0, 24, 48 and 100 cycles).

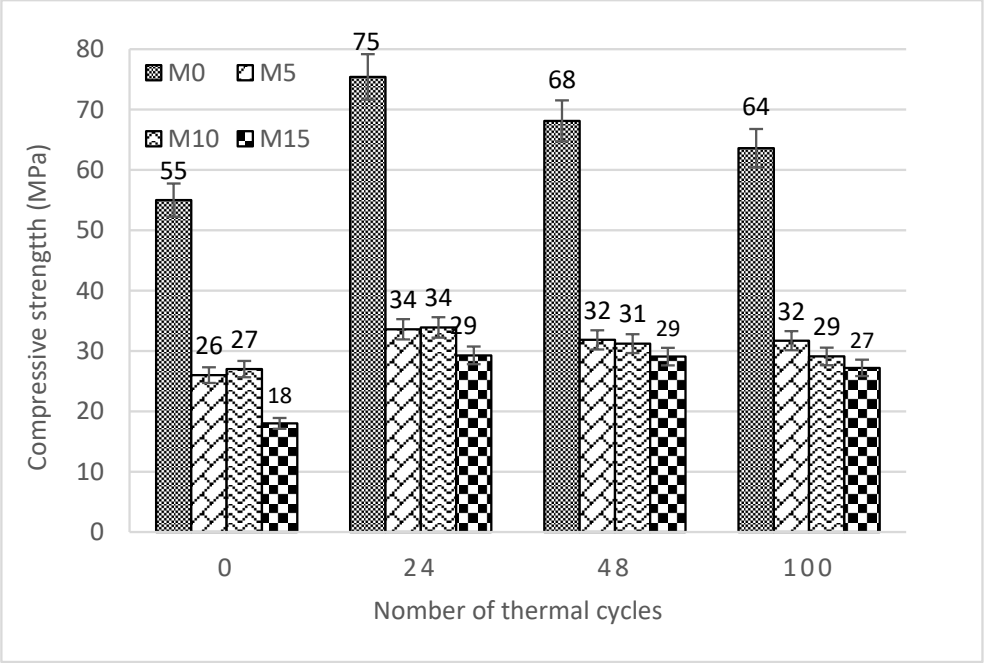


**Figure 21.** Compressive strength of mortars as a function of thermal aging cycles.

A significant increase in compressive strength of all mortar samples is noticed after 24 cycles, a slight decrease occurred between 48 and 100 cycles. This mechanical performance improvement after 24 cycles should be related to the thermal activation of hydration reactions, increasing the hydration kinetics of mortars. For mortars incorporating SS-PCM, there is a convergence towards the similar value of around 30 MPa after 100 cycles. Overall, the Figure 21 shows the mechanical stability of SS-PCM composite mortars over the heat storage cycles (until 100 cycles). This mechanical stability should be explained by the volume stability of SS-PCM during phase change. Indeed, unlike classic solid-liquid PCM (SL-PCM) as paraffin with solid-liquid transition phase (volume instability), the SS-PCM have the advantage of a stable solid-solid transition phase (volume stability). Hence, the volume stability of SS-PCM during the storage-distorage cycle allowed to avoid stress and cracking into the mortar skeleton. Furthermore, it should be noted that this study should be conducted over a larger number of cycles (200 cycles) to be more representative. For supporting structure applications in building, it is important to keep mechanical stability over heat storage cycles.

## 4. Conclusions

The influence of SS-PCM incorporations on properties and durability of mortars was examined. The rheological, structural, mechanical and thermal properties of SS-PCM mortars were measured and analyzed. Then, the durability study allowed assessing the volume (drying shrinkage), chemical (carbonation) and mechanical stabilities (over thermal storage cycles). The results showed that:

- The increase of SS-PCM content in the fresh mortar induces a better workability and increases the total porosity, hence a drop in mechanical strength and thermal

conductivity. However, the mechanical performance of SS-PCM composite mortars remains sufficient (27–18 MPa) for most building applications.

- The drying shrinkage amplitude decreases with its SS-PCM content. This result should be related to the compressibility of the SS-PCM amortizing the local capillary pressure, leading to less measurable bulk deformation.
- An increase in mechanical strength with the carbonation rate was noted. The mechanical stability of SS-PCM composite mortars over the heat storage cycles is confirmed. This should be explained by the volume stability of SS-PCM during phase change unlike classic SL-PCM.

The advantage of this innovative SS-PCM compared to the existing SL-PCM is its ability to store high thermal energy with a better durability thanks to its volume stability during solid-solid phase change. So, this storage material could be a solution for the durability problems inhibiting the use of phase change materials in building sector. The SS-PCM mortar was suitable for masonry coating, masonry bricks, roof coating, covering panels, etc. This allow to improve the thermal inertia of the building, thus avoiding sudden changes in the indoor temperature, all while maintaining the supporting structure capacity.

**Author Contributions:** Conceptualization: Y.R., K.N., L.P. and Z.E.A.T.; Methodology: Y.R., K.N., L.P., Z.E.A.T., A.C. and Y.M.; Formal analysis: Y.R., K.N., L.P., Z.E.A.T., A.C. and Y.M.; Investigation: Y.R. and K.N.; Writing—original draft: Y.R. and K.N.; Visualization: Y.R. and K.N.; Editing: Y.R. and K.N.; Writing—review: L.P., Z.E.A.T., A.C. and Y.M.; Supervision: Y.M. and K.N. All authors have read and agreed to the published version of the manuscript.

**Funding:** This research received no external funding.

**Institutional Review Board Statement:** Not applicable.

**Informed Consent Statement:** Not applicable.

**Data Availability Statement:** The data presented in this study are available on request from the corresponding author.

**Acknowledgments:** The SS-PCM are supplied by the "Laboratoire GEC" of Cergy Paris University (France). The SEM analyses were carried out in the "Microscopies & Analyses" imaging facility, Federation I-Mat (FR4122) of the CY Cergy Paris University. The mercury intrusion porosimetry (MIP) was performed in the "Laboratoire Matériaux et Durabilité des Constructions" of the Toulouse University (France).

**Conflicts of Interest:** The authors declare no conflict of interest.

## References

1. Fallahi, A.; Guldentops, G.; Tao, M.; Granados-Focil, S.; Van Dessel, S. Review on solid-solid phase change materials for thermal energy storage: Molecular structure and thermal properties. *Appl. Therm. Eng.* **2017**, *127*, 1427–1441. [CrossRef]
2. Ndiaye, K.; Ginestet, S.; Cyr, M. Thermal energy storage based on cementitious materials: A review. *AIMS Energy* **2018**, *6*, 97–120. [CrossRef]
3. Šavija, B. Smart Crack Control in Concrete through Use of Phase Change Materials (PCMs): A Review. *Materials* **2018**, *11*, 654. [CrossRef] [PubMed]
4. Liu, L.; Li, J.; Deng, Y.; Yang, Z.; Huang, K.; Zhao, S. Optimal design of multi-layer structure composite containing inorganic hydrated salt phase change materials and cement: Lab-scale tests for buildings. *Constr. Build. Mater.* **2021**, *275*, 122125. [CrossRef]
5. Soares, N.; Costa, J.J.; Gaspar, A.R.; Santos, P. Review of passive PCM latent heat thermal energy storage systems towards buildings' energy efficiency. *Energy Build.* **2013**, *59*, 82–103. [CrossRef]
6. Baetens, R.; Jelle, B.P.; Gustavsen, A. Phase change materials for building applications: A state-of-the-art review. *Energy Build.* **2010**, *42*, 1361–1368. [CrossRef]
7. Jayalath, A.; Mendis, P.; Gammampila, R.; Aye, L. Applications of phase change materials in concrete for sustainable built environment: A Review. In Proceedings of the International Conference on Structural Engineering, Construction and Management, Kandy, Sri Lanka, 16–18 December 2011. Available online: http://dl.lib.mrt.ac.lk/handle/123/9349 (accessed on 8 March 2023).
8. Snoeck, D.; Priem, B.; Dubruel, P.; De Belie, N. Encapsulated Phase-Change Materials as additives in cementitious materials to promote thermal comfort in concrete constructions. *Mater. Struct.* **2014**, *49*, 225–239. [CrossRef]
9. Adesina, A.; Awoyera, P.; Sivakrishna, A.; Kumar, K.R.; Gobinath, R. Phase change materials in concrete: An overview of properties. *Mater. Today Proc.* **2020**, *27*, 391–395. [CrossRef]

10. Ren, M.; Wen, X.; Gao, X.; Liu, Y. Thermal and mechanical properties of ultra-high performance concrete incorporated with microencapsulated phase change material. *Constr. Build. Mater.* **2021**, *273*, 121714. [CrossRef]
11. Asimakopoulou, E.K.; Kolaitis, D.I.; Founti, M.A. Fire safety aspects of PCM-enhanced gypsum plasterboards: An experimental and numerical investigation. *Fire Saf. J.* **2015**, *72*, 50–58. [CrossRef]
12. Essid, N.; Loulizi, A.; Neji, J. Compressive strength and hygric properties of concretes incorporating microencapsulated phase change material. *Constr. Build. Mater.* **2019**, *222*, 254–262. [CrossRef]
13. Šavija, B.; Zhang, H.; Schlangen, E. Influence of Microencapsulated Phase Change Material (PCM) Addition on (Micro) Mechanical Properties of Cement Paste. *Materials* **2017**, *10*, 863. [CrossRef]
14. Halamickova, P.; Detwiler, R.J.; Bentz, D.P.; Garboczi, E.J. Water permeability and chloride ion diffusion in portland cement mortars: Relationship to sand content and critical pore diameter. *Cem. Concr. Res.* **1995**, *25*, 790–802. [CrossRef]
15. Dehdezi, P.K.; Hall, M.R.; Dawson, A.R.; Casey, S.P. Thermal, mechanical and microstructural analysis of concrete containing microencapsulated phase change materials. *Int. J. Pavement Eng.* **2013**, *14*, 449–462. [CrossRef]
16. Hunger, M.; Entrop, A.G.; Mandilaras, I.; Brouwers, H.J.H.; Founti, M. The direct incorporation of microencapsulated Phase Change Materials in the concrete mixing process. In Proceedings of the CMS 2009 Conference on Life Cycle Design of Building Systems and Materials, Enschede, The Netherlands, 12–15 June 2009. Available online: https://www.academia.edu/22180396 (accessed on 8 September 2023).
17. Wei, Z.; Falzone, G.; Wang, B.; Thiele, A.; Puerta-Falla, G.; Pilon, L.; Neithalath, N.; Sant, G. The durability of cementitious composites containing microencapsulated phase change materials. *Cem. Concr. Compos.* **2018**, *81*, 66–76. [CrossRef]
18. Drissi, S.; Ling, T.-C. Thermal and durability performances of mortar and concrete containing phase change materials. *IOP Conf. Ser. Mater. Sci. Eng.* **2018**, *431*, 062001. [CrossRef]
19. Jiang, Y.; Ding, E.; Li, G. Study on transition characteristics of PEG/CDA solid–solid phase change materials. *Polymer* **2002**, *43*, 117–122. [CrossRef]
20. Alkan, C.; Günther, E.; Hiebler, S.; Ensari, Ö.F.; Kahraman, D. Polyurethanes as solid-solid phase change materials for thermal energy storage. *Sol. Energy* **2012**, *86*, 1761–1769. [CrossRef]
21. Tang, B.; Yang, Z.; Zhang, S. Poly(polyethylene glycol methyl ether methacrylate) as Novel Solid-Solid Phase Change Material for Thermal Energy Storage. *J. Appl. Polym. Sci.* **2012**, *125*, 1377–1381. [CrossRef]
22. Yanshan, L.; Shujun, W.; Hongyan, L.; Fanbin, M.; Huanqing, M.; Wangang, Z. Preparation and characterization of melamine/formaldehyde/polyethylene glycol crosslinking copolymers as solid–solid phase change materials. *Sol. Energy Mater. Sol. Cells* **2014**, *127*, 92–97. [CrossRef]
23. Harlé, T.; Ledesert, B.; Nguyen, T.M.G.; Hebert, R.; Melinge, Y. Phase-Change Material for Storing Thermal Energy, Manufacturing Method and Uses of Such a Material. WO 2017198933 A1, 23 November 2017. Available online: https://patents.google.com/patent/WO2017198933A1 (accessed on 2 October 2023).
24. Plancher, L.; Pierre, A.; Nguyen, G.T.M.; Hébert, R.L.; Ledésert, B.A.; Di Martino, P.; Mélinge, Y. Rheological Behaviour of Cementitious Materials Incorporating Solid–Solid Phase Change Materials. *Materials* **2022**, *15*, 20. [CrossRef] [PubMed]
25. NF EN 196-1, Méthodes D'essais des Ciments, Partie 1: Détermination des Résistances Mécaniques 2016. Available online: https://www.boutique.afnor.org/norme/nf-en-196-1/methodes-d-essais-des-ciments-partie-1-determination-des-resistances/article/866862/fa184622 (accessed on 12 October 2023).
26. Benabed, B.; Kadri, E.-H.; Azzouz, L.; Kenai, S. Properties of self-compacting mortar made with various types of sand. *Cem. Concr. Compos.* **2012**, *34*, 1167–1173. [CrossRef]
27. The French National Research Project PERFDUB. Approche Performantielle de la Durabilité des Ouvrages en Béton. Available online: https://www.perfdub.fr/en/ (accessed on 14 October 2020).
28. Zhang, Y.; Yang, Z.; Ye, G. Dependence of unsaturated chloride diffusion on the pore structure in cementitious materials. *Cem. Concr. Res.* **2020**, *127*, 105919. [CrossRef]
29. Samson, G.; Phelipot-Mardelé, A.; Lanos, C.; Alogla, K.; Weekes, L.; Augusthus-Nelson, L.; Arora, S.; Singh, S.P.; Zhang, J.; Ma, H.; et al. A review of thermomechanical properties of lightweight concrete. *Mag. Concr. Res.* **2017**, *69*, 201–216. [CrossRef]
30. Narain, J.; Jin, W.; Ghandehari, M.; Wilke, E.; Shukla, N.; Berardi, U.; El-Korchi, T.; Van Dessel, S. Design and Application of Concrete Tiles Enhanced with Microencapsulated Phase-Change Material. *J. Arch. Eng.* **2016**, *22*, 05015003. [CrossRef]
31. Cao, V.D.; Pilehvar, S.; Salas-Bringas, C.; Szczotok, A.M.; Rodriguez, J.F.; Carmona, M.; Al-Manasir, N.; Kjøniksen, A.-L. Microencapsulated phase change materials for enhancing the thermal performance of Portland cement concrete and geopolymer concrete for passive building applications. *Energy Convers. Manag.* **2017**, *133*, 56–66. [CrossRef]
32. Lura, P.; Jensen, O.M.; van Breugel, K. Autogenous shrinkage in high-performance cement paste: An evaluation of basic mechanisms. *Cem. Concr. Res.* **2003**, *33*, 223–232. [CrossRef]
33. Grasley, Z.C.; Leung, C.K. Desiccation shrinkage of cementitious materials as an aging, poroviscoelastic response. *Cem. Concr. Res.* **2011**, *41*, 77–89. [CrossRef]
34. Di Bella, C.; Wyrzykowski, M.; Lura, P. Evaluation of the ultimate drying shrinkage of cement-based mortars with poroelastic models. *Mater. Struct.* **2017**, *50*, 52. [CrossRef]
35. Neville, A.M. *Properties of Concrete*, 4th ed.; Pearson Higher Education, Prentice Hall: Englewood Cliffs, NJ, USA, 1995. Available online: https://www.technicalbookspdf.com/properties-of-concrete-fifth-edition-a-m-neville/ (accessed on 28 November 2023).

36. Chuang, C.-W.; Chen, T.-A.; Huang, R. Effect of Finely Ground Coal Bottom Ash as Replacement for Portland Cement on the Properties of Ordinary Concrete. *Appl. Sci.* **2023**, *13*, 13212. [CrossRef]
37. Pacheco-Torgal, F.; Labrincha, J.; Leonelli, C.; Palomo, A.; Chindaprasirt, P. *Handbook of Alkali-Activated Cements, Mortars and Concretes*, 1st ed.; Abington Hall: Cambridge, UK, 2015. Available online: https://www.sciencedirect.com/book/9781782422761 (accessed on 5 October 2023).
38. Stefan, L.; Boulay, C.; Torrenti, J.-M.; Bissonnette, B.; Benboudjema, F. Influential factors in volume change measurements for cementitious materials at early ages and in isothermal conditions. *Cem. Concr. Compos.* **2018**, *85*, 105–121. [CrossRef]
39. Gilbert, R. *Time Effects in Concrete Structures*; Elsevier: Amsterdam, The Netherlands, 1988. Available online: https://trid.trb.org/view/311317 (accessed on 3 February 2024).
40. Rusch, H.; Jungwirth, D.; Hilsdorf, D.H. *Creep and Shrinkage, Their Effect on the Behaviour of Concrete Structures*; Springer: New York, NY, USA, 1983. Available online: https://www.springer.com/gp/book/9781461254263 (accessed on 7 September 2023).
41. Medvedev, V.; Pustovgar, A.; Adamtsevich, A.; Adamtsevich, L. Concrete Carbonation of Deep Burial Storage Constructions under Model Aging Conditions. *Buildings* **2023**, *14*, 8. [CrossRef]